

Geophysical Research Letters



RESEARCH LETTER

10.1029/2020GL090690

Key Points:

- Cold ions in the inflow region affect reconnection on both micro- and macro-scales
- The micro-macro coupling of mass-loading is mediated by the cold ion inertia
- Cold and warm ions are counter streaming close to the ion diffusion region boundary

Correspondence to:

S. F. Spinnangr,
susanne.spinnangr@uib.no

Citation:

Spinnangr, S. F., Hesse, M., Tenfjord, P., Norgren, C., Kolstø, H. M., Kwagala, N. K., & Jørgensen, T. M. (2021). The micro-macro coupling of mass-loading in symmetric magnetic reconnection with cold ions. *Geophysical Research Letters*, 48, e2020GL090690. <https://doi.org/10.1029/2020GL090690>

Received 4 SEP 2020

Accepted 14 JUN 2021

The Micro-Macro Coupling of Mass-Loading in Symmetric Magnetic Reconnection With Cold Ions

Susanne F. Spinnangr¹ , Michael Hesse² , Paul Tenfjord¹ , Cecilia Norgren¹ , Håkon M. Kolstø¹ , Norah K. Kwagala¹ , and Therese M. Jørgensen² 

¹Space Plasma Physics Group, University of Bergen, Bergen, Norway, ²NASA Ames Research Center, Mountain View, CA, USA

Abstract We investigate how magnetic reconnection is influenced by an inflow of a dense cold ion population. We compare two 2.5D Particle-In-Cell simulations, one containing the cold population and one without. We find that the cold population influences the reconnection process on both global and kinetic scales, and that the dominant contribution can be explained through mass-loading. We provide an analysis of how these multiscale changes are related through kinetic processes in the ion diffusion region, the so-called micro-macro coupling of mass-loading. The inertia of the cold ion population is found to be the significant link that connects the changes on different scales. The cold and warm populations exhibit counter streaming behavior when and after the ion diffusion region reorganizes itself in response to the arrival of the cold population. This signature of the cold population should be observable by spacecraft observatories such as MMS.

Plain Language Summary We investigate how magnetic reconnection is influenced by a dense inflow of cold ions. We find that the cold ions influence the reconnection process on both large and small scales, and that these are connected through the cold ion inertia. We also see cold and warm ions moving in opposite directions close to the reconnection site, which should be observable by spacecraft observatories.

1. Introduction

Magnetic reconnection is a process where energy stored in magnetic fields gets converted into kinetic and thermal energy in the plasma, caused by a macroscopic change in the magnetic topology. It occurs in plasma environments in space, such as the Sun and the magnetosphere, as well as in plasma laboratories and fusion reactors on Earth (Yamada et al., 2010). In a plasma, the magnetic field is closely coupled to the dynamics of the plasma particles. How the magnetic reconnection process evolves is therefore highly influenced by the constituents of the plasma in the inflow regions. Spacecraft observations in the magnetosphere show, that in addition to the warm plasma populations that form current sheets in magnetic field reversal regions, populations of cold ions of ionospheric origin are commonly present, and might even constitute the dominant particle species in the system (André & Cully, 2012; André, Li, & Eriksson, 2015; Fuselier, Burch, Mukherjee, et al., 2017; Walsh et al., 2014). Usually, the thermal energies of the warm plasma populations are in the range of a few hundred eV to several keV, while the cold populations typically have energies of a few eV (André, Li, Toledo-Redondo, et al., 2016), although cold ions of larger energy ranges as well as of different densities and origins have been observed in various regions of the magnetosphere (Fuselier, Burch, Cassak, et al., 2016; Fuselier, Burch, Mukherjee, et al., 2017). Multiple previous studies and observations have shown that the presence of additional plasma populations has an impact on characteristic temporal and spatial scales associated with the diffusion region (Alm et al., 2019; André, Li, Toledo-Redondo, et al., 2016; Dargent, Aunai, Lavraud, Toledo-Redondo, & Califano, 2019; Dargent, Aunai, Lavraud, Toledo-Redondo, Shay, et al., 2017; Divin et al., 2016; Toledo-Redondo, André, et al., 2016; Toledo-Redondo, Vaivads, et al., 2015). These scales include the Larmor radius, $r_{Ls} = \frac{m_s v_{Ts}}{q_s B}$,

where v_{Ts} is the perpendicular velocity of the particle. As a gyrating particle with smaller Larmor radius will remain frozen in for a longer time when approaching the X-point, multiple diffusion regions exist for the different particle populations. Such multiscale diffusion regions (more than two layers) have become a common feature in both Particle-In-Cell (PIC) simulations and observations (e.g., Alm et al. 2019; André, Li, Toledo-Redondo,

© 2021. The Authors.

This is an open access article under the terms of the [Creative Commons Attribution License](https://creativecommons.org/licenses/by/4.0/), which permits use, distribution and reproduction in any medium, provided the original work is properly cited.

et al., 2016; Dargent, Aunai, Lavraud, Toledo-Redondo, & Califano, 2020; Divin et al. 2016; Toledo-Redondo, André, et al., 2016; Toledo-Redondo, Vaivads, et al., 2015). One of the questions that remain unresolved regarding magnetic reconnection is how it stops. Since multiple plasma species have been shown to influence important features of the reconnection process, such as the reconnection rate and the Hall physics (Alm et al., 2019; André, Li, Toledo-Redondo, et al., 2016; Tenfjord, Hesse, & Norgren, 2018), understanding how reconnection responds to different inflow conditions will aid in answering this question. In this study we investigate how mass-loading the inflow regions with a large cold ion population modifies the evolution of the magnetic reconnection process. On macro-scales we expect to see a reduction in the reconnection rate, which will slow the reconnection process down. However, how this couples to the micro-scale dynamics in the diffusion region is not understood. We show that the inertia of the newly arriving cold ions play a vital role in mediating the changes on different scales. Signatures of this interaction that can be observable with spacecraft observatories such as the Magnetospheric Multiscale Mission (MMS) are briefly discussed.

We describe the simulations used for this study in Section 2. In Section 3, we describe the macro-scale effects of cold ion mass-loading on the reconnection rate. In Sections 4 and 5, we take a closer look at how this is related to the micro-scale dynamics of the ion diffusion region, and in Section 6 we summarize and discuss implications of our results.

2. Simulation Setup

In this study we compare two 2.5D PIC simulations, both corresponding to a symmetric tail reconnection event with no guide field. Our code is a parallelized evolution of the one described in (Hesse, Schindler, et al., 1999). The first simulation contains only warm plasma, which we call the baseline run. Similar setups have previously been used to model a variety of different reconnection problems (e.g., Hesse, Birn, & Kuznetsova, 2001; Tenfjord, Hesse, & Norgren, 2018; Tenfjord, Hesse, Norgren, Spinnangr, & Kolstø, 2019). In another simulation we call the cold run, we add a population of cold ions to the baseline setup, $4.5d_i$ outside of the current sheet. Lengths are normalized to the ion inertial length, $d_i = \frac{c}{\omega_{pi}}$, where $\omega_{pi} = \sqrt{\frac{4\pi n_0 e^2}{m_i}}$, $m_i =$ ion mass, $e =$ elementary charge) is the ion plasma frequency and c is the speed of light. Densities are normalized to the Harris current sheet density, n_0 , and velocities are normalized to the ion Alfvén velocity. Our initial magnetic field and current sheet configurations are 2-D Harris type configurations, with magnetic field $B_x = B_0 \tanh\left(\frac{z}{\lambda}\right)$, where $\lambda = 2d_i$ is the halfwidth of the current layer, and with an additional localized perturbation creating an X-point. Additionally, a uniform density distribution of 0.2 of warm ions is added to the whole simulation domain. Time is normalized to the inverse ion cyclotron frequency, $\Omega_i^{-1} = \frac{m_i}{eB_0}$, and we employ a time step of $\omega_{pe}\delta t = 0.5 \left(\omega_{pe} = \omega_{pi} \sqrt{\frac{m_i}{m_e}} \right)$. A total of 9.6×10^9 macroparticles are used, with mass ratio $\frac{m_i}{m_e} = 25$. For the upper and lower boundary conditions we employ specular reflection, while the left and right boundary conditions are periodic at $x = x_{\min}$ and $x = x_{\max}$. The out-of-plane electric field is set to zero in order to ensure flux conservation in the simulation domain. The size of the simulation domain is $410 \times 50 d_i$, divided into a grid of $6,400 \times 1,600$ cells. In the cold run, a uniform density distribution of 0.4 of cold ions is added to the inflow at $|z| \geq 4.5$. The initial temperature of the cold populations is set to zero. In Figure 1 we show an overview of the evolution of the two runs. The cold ions arrive at the reconnection site at time = 98, which corresponds to the time of peak reconnection rate in the cold run.

3. The Reconnection Rate

The reconnection rate is a measure of the speed at which the magnetic flux changes on large-scale, defined as

$$\frac{d}{dt} \Phi_{rec} = \frac{d}{dt} \int \vec{B} \cdot \vec{n} dA = \frac{d}{dt} \int B_z dx \quad (1)$$

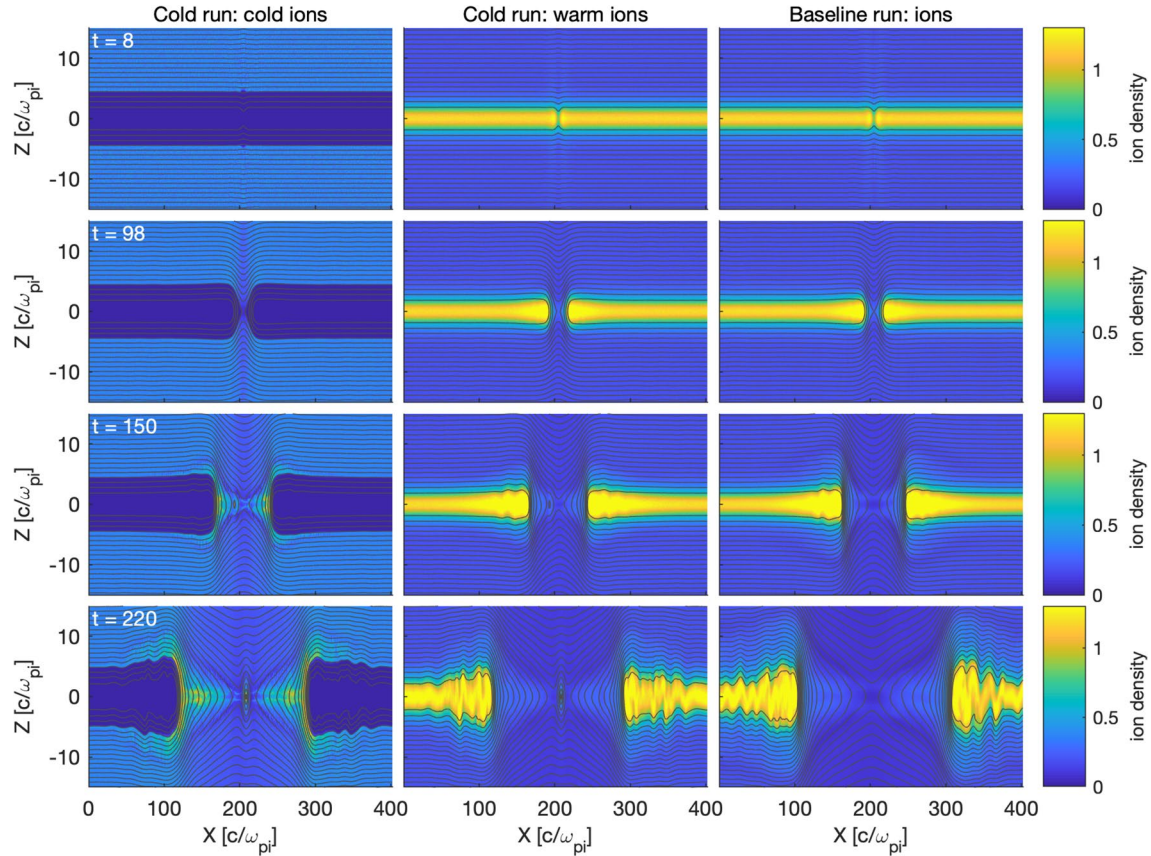


Figure 1. Time evolution of the ion density and the in-plane magnetic field contours in the two runs. (Left) Cold and (middle) warm ion density in the cold run. (Right) Total ion density in the baseline run. By comparing the x -position of the dipolarization front in the middle and right columns we see that the cold run is reconnecting slightly slower than the baseline run.

where Φ_{rec} is the reconnected flux, \vec{B} is the magnetic field, and \vec{n} is the normal vector of the reference surface.

Figure 2 shows the reconnection rate of both the cold and baseline run, plotted as a function of time and the fractional reduction of magnetic energy density in the system. As expected, since the cold run is mass-loaded, it shows a significantly reduced rate compared to the baseline when the cold ions become involved at time = 98. The presence of cold ions in the inflow region makes the flux tubes more inert and slows down the reconnection process. When comparing the two runs it is therefore more appropriate to compare them when they are at the same stage of the evolution, meaning when they have converted the same amount of magnetic energy, rather than at the same point in time. This is plotted Figure 2b. Figure 2c shows the reconnection rates rescaled for the effect of mass-loading. The reconnection electric field is expected to scale with the factor $B_x V_A$ (Cassak et al., 2017; Comisso & Bhattacharjee, 2016; Liu et al., 2017), with both B_x and V_A measured in the inflow region in close vicinity to the diffusion region. When we mass-load the inflow region we effectively reduce the Alfvén velocity. By dividing the reconnection rate by this scaling factor, we should therefore remove the effect of mass-loading on the rate. The values for the magnetic field and density needed to calculate this scaling factor are averaged over $|z| = 4 d_i \pm 1 d_i$ above and below the X-point. We find the average again of the two values calculated above and below the current sheet. These double-averaged values become the final values used in the scaling factor. Averaging in this way reduces the effect of grid size fluctuations in the ion density. Both the baseline and the cold run have been rescaled in the same way to account for the changes in magnetic flux and density inflow as the reconnection process evolves. Figure 2c shows that the reconnection rates of the two runs are comparable after rescaling. The cold run ends up with a slightly higher rate than the baseline run because the mass-loading scaling assumes the cold ions are distributed homogeneously in the system. Since we only insert them outside $|z| \geq 4.5 d_i$, the initial current sheet

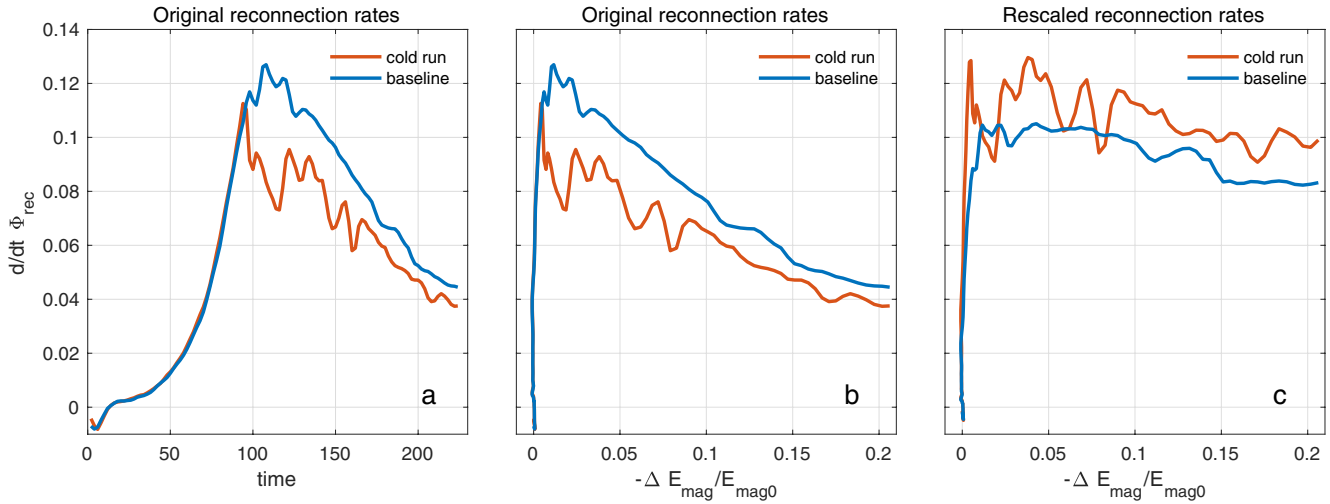


Figure 2. (a) Original reconnection rate of both runs as a function of time and (b) the fractional change in magnetic energy density. (c) Both reconnection rates after they have been rescaled to account for mass-loading.

is less inert than the scaling assumes, which results in a slightly higher rate. Nevertheless, we can conclude that the decrease in the reconnection rate in the cold run is dominated by the mass-loading effect. This is consistent with similar studies, such as (Dargent, Aunai, Lavraud, Toledo-Redondo, & Califano, 2020; Divin et al., 2016; Tenfjord, Hesse, Norgren, Spinnangr, Kolstø, & Kwagala, 2020). Based on a Sweet-Parker analysis of magnetic reconnection, we can set the outflow velocity of the plasma particles to the Alfvén velocity,

$$v_{out}^2 = v_A^2 = \frac{B^2}{\mu_0 \rho} \quad (2)$$

where ρ is the incoming mass density on both sides of the diffusion region, and B is the magnetic field at the same location (Vasyliunas, 1975). From mass conservation it follows that the mass flow into the diffusion region must equal the outflow. Defining the height and width of the diffusion region as δ and L respectively, and assuming incompressible flow ($\nabla \cdot \mathbf{v} = 0$), steady-state mass conservation reveals the following well established relation between the aspect ratio of the diffusion region and the flow velocities

$$\frac{\delta}{L} \sim \frac{v_{in}}{v_{out}} = \frac{v_{in}}{v_A} \quad (3)$$

The velocity ratio in this equation is another common expression for the reconnection rate (Vasyliunas, 1975). Hence, when the reconnection rate is reduced by mass-loading, the aspect ratio of the diffusion region must experience a similar reduction if the mass flow is incompressible. The reconnection rate is often referred to as a macro-scale feature of the reconnection process, since it is a large-scale effect. The aspect ratio of the diffusion region is on kinetic scales, and its reduction is therefore a micro-scale effect. How these micro- and macro-scale effects are coupled is a long-standing question in magnetic reconnection which we will try to shed some light on in the following sections where we take a closer look at the ion diffusion region.

4. Scale Change of the Ion Diffusion Region

When the reconnection process evolves, the cold ion population will be energized and both the cold and the warm ions will participate. Earlier studies have shown that multiple plasma species partition the diffusion region, where the cold ion diffusion region lies between that of the warm ions and the electrons (Alm et al., 2019; André, Li, Toledo-Redondo, et al., 2016; Dargent, Aunai, Lavraud, Toledo-Redondo, & Califano, 2019; Divin et al., 2016; Toledo-Redondo, André, et al., 2016). However, researching the scaling

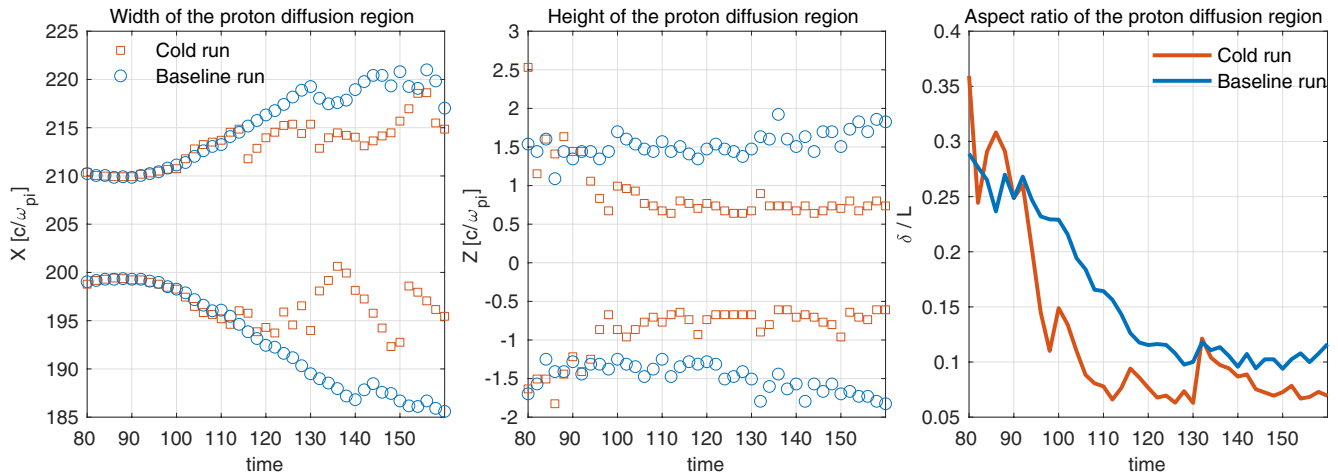


Figure 3. The height, width and aspect ratio of the total ion diffusion region for both runs. The baseline run continues expanding in both the inflow and outflow direction through the full time interval. In the cold run, the expansion in the width is reduced, along with a clear reduction in the height as the cold ions reach the reconnection site.

of the reconnection rate with the effect of mass-loading should involve the total ion population. Like in fluid models, the aspect ratio of the ion diffusion region is expected to scale with the reconnection rate also in kinetic plasmas. In this analysis, we therefore choose to treat the combination of the two ion species to find effective ion diffusion region dimensions as that region transitions from being fully dominated by the warm ion species to being influenced by the cold species. We only care about the dynamics of this combined ion aspect ratio, not its actual size, and we therefore use simple methods that give an estimate of the dimensions. In the inflow direction, we have defined the limit where the non-ideal terms in Ohm's law for the reconnection electric (Equation 6) field become dominant as a proxy for the diffusion region height. We identify the point above and below the X-point where $v_z B_x = 0.5 E_y$, which defines the limit where E_y goes from being dominated by the frozen in $\mathbf{v} \times \mathbf{B}$ drift to being mostly diffusive. In the outflow direction the dynamics are more complicated, and we therefore employ a different method. There we have defined the limit where the local thermal ion Larmor radius becomes equal to the distance from the X-point as a proxy for the diffusion region width (Divin et al., 2016). This is similar to comparing the bounce width of the ions with the distance from the X-point.

Figure 3 shows the diffusion region width (L), height (δ), and aspect ratio (δ/L), all plotted around the time interval where the cold ions arrive at the reconnection site. There is some noise in the estimation of the diffusion region width in the cold run, caused by a high rate of island production, which can affect the calculation of the local Larmor radius. In order to avoid as much interference from islands as possible, the locations in this figure are therefore selected manually. In this way, we have made sure that the chosen locations are as close to the real boundary of the diffusion region width as possible, and not just an artificial boundary caused by an island moving through the diffusion region. However, the noise is still significant enough that we only look at the overall behavior through the full time interval. The baseline behaves as expected, with gradually increasing width of the diffusion region as reconnection proceeds. In Figure 3 we see that when the cold ions start to get involved around time = 96, the diffusion region height experiences a reduction of about 50%. We also see a reduction in the expansion rate of the width at a later time. The net effect of the cold ions on the diffusion region can be seen in the aspect ratio. Figure 3 shows that the aspect ratio is significantly reduced during the time interval when the cold ions arrive before it stabilizes slightly below $\delta/L = 0.1$. A similar reduction and stabilization is also present in the baseline run due to the expansion in the outflow direction. However, since the baseline does not experience any reduction in the diffusion region height, the drop is slower and less dramatic. In both runs, the stabilization around $\delta/L = 0.1$ coincides with the stabilization of the rescaled reconnection rate around the same value (not shown). This value for the reconnection rate has been shown to be common between a variety of different reconnecting systems (Cassak et al., 2017; Comisso & Bhattacharjee, 2016; Liu et al., 2017).

To investigate the changes on micro-scales further, we take a closer look at the reconnection electric field, E_y , which at the X-line is directly proportional to the reconnection rate. If we assume that the ions are frozen in at the edges of the diffusion region, and that E_y is the same at both the inflow and outflow edge, we obtain the following relation:

$$v_{in}B_x = v_{out}B_z \quad (4)$$

We use $\nabla \cdot B = 0$ and Equation 3 to rewrite this in an explicit form for the electric field:

$$E_y \sim v_A B_z \sim v_A B_x \frac{\delta}{L} \quad (5)$$

This directly relates the reconnection electric field, that is, the reconnection rate, to the the Alfvén velocity and the aspect ratio of the diffusion region, which are both affected by mass-loading. In the following section, we will investigate how micro-scale processes in the ion diffusion region caused by the inflow of dense, cold plasma leads to a reduction in E_y , and thereby a macro-scale reduction in the reconnection rate.

5. Role of Cold Ion Inertia

In order to investigate how E_y is being reduced as the cold ions arrive, we take a closer look at all the contributing terms as a function of z through the X-point. We express E_y through the generalized Ohm's law

$$E_y = \left(-\vec{v} \times \vec{B} + \frac{1}{qn} \nabla \cdot P + \frac{m}{q} \left(\vec{v} \cdot \nabla \vec{v} + \frac{\partial \vec{v}}{\partial t} \right) \right)_y \quad (6)$$

The first term on the right hand side of this equation describes the frozen in motion, the second term describes the contribution from the divergence of the pressure, and the third and fourth term describe the contribution from the convective and temporal inertia respectively. In Figure 4, this is plotted for both the cold and baseline run for different points in time. For time = 90, the cold ions have not yet arrived at the reconnection site. At time = 98, the incoming cold fronts are just meeting at the X-point, while at time = 104 the cold population contributes about one third of the total density at the X-point. By comparing the cold run and the baseline runs, we see a significant contribution from the temporal inertia when the cold ions are involved, which is not present in the baseline run. We also see that this contribution disappears at time = 104, and the two runs become more similar. The reconnection electric field is reduced by this inertia contribution during the transition when the cold ions go from not being involved to being fully involved in the reconnection process. During this transition period the reconnection process reorganizes itself on a kinetic level to incorporate the effects of the incoming additional mass density. In order to investigate how this happens, we take a closer look at the dynamics of the cold ions as they enter the diffusion region.

In Figure 5, we have plotted the density and the y -component of the velocity in the cold run for the total, warm and cold ion population as a function of z through the X-point. We show this for the same, and two additional intermediate, points in time as we investigated in Figure 4. During the same time interval where the negative inertia contribution to the reconnection electric field is significant, Figure 5 shows that the cold ions have a negative v_y , while the warm ions have a positive v_y . Comparing the changes in these velocities we see that the reduction of the total ion velocity causing the negative inertia contribution to E_y is due to the cold ions. When the cold ions approach the X-point, the system has already been reconnecting with the warm plasma for some time, and the Hall electric field has been established. The cold ions move toward the X-point like two density fronts and they are accelerated by the Hall-field. They are then turned by B_x and gain a negative v_y , which has a significant effect on the total ion v_y in the diffusion region.

Later, when a large enough fraction of the cold population has had the time to demagnetize and participate in the bouncing motion between the opposite B_x regions, they have established a large enough pressure gradient in the z -direction to exhibit diamagnetic drift. This drift is in the positive v_y direction, and does eventually become dominant. In

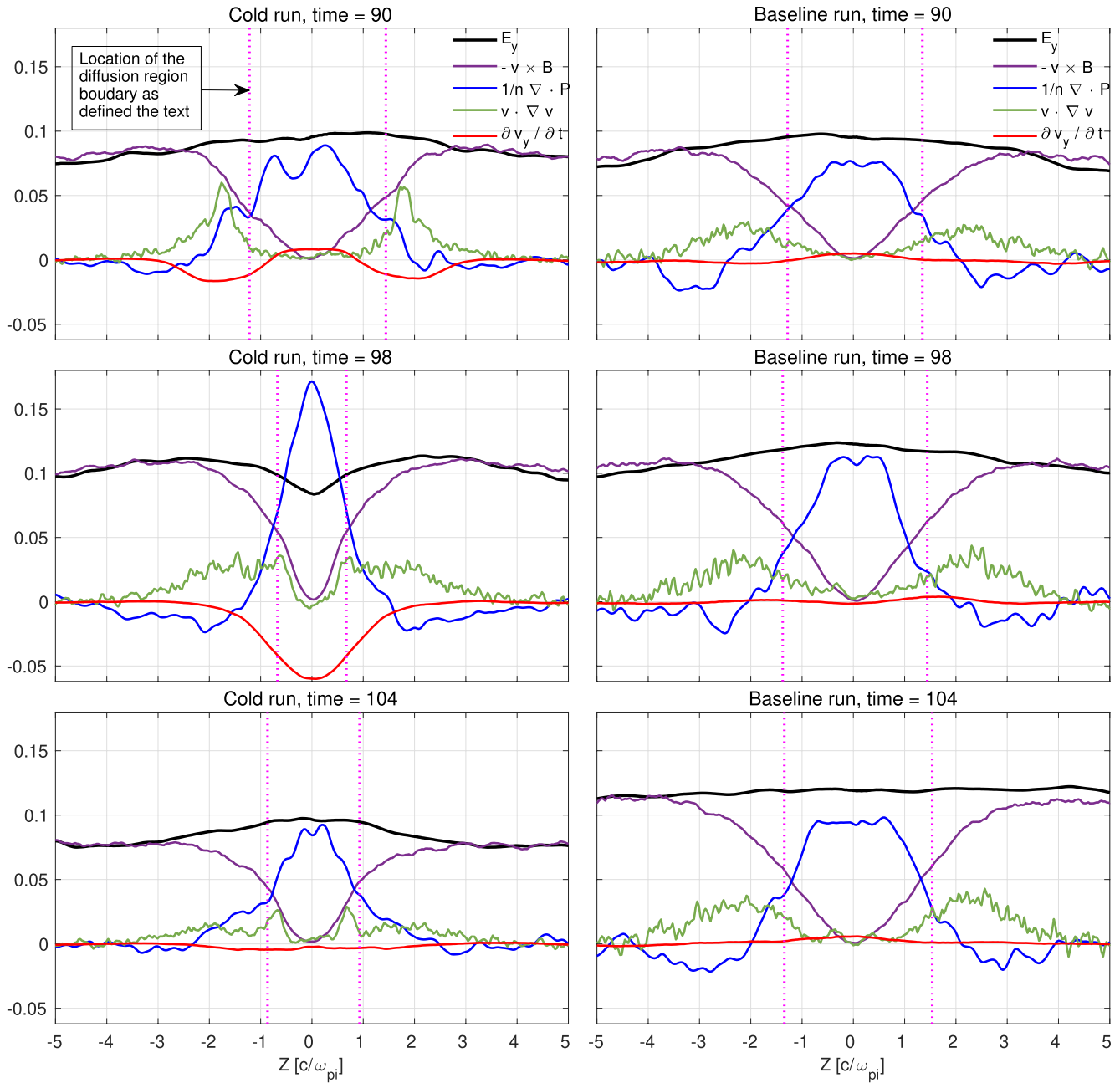


Figure 4. The contributing terms to the reconnection electric field as described in Equation 6 ($q = m = 1$), as a function of z through the X-point before, during and after the cold ions arrive at the reconnection site. The temporal inertia (red) has a significant contribution in the cold run, but a negligible contribution in the baseline run.

sum, the interaction of these oppositely directed process causes a negative y -directed inertia only in the transition before a large enough density of the cold ions have had enough time to exhibit diamagnetic drift.

6. Discussion and Summary

In this work we have investigated the effect of mass-loading by a cold ion population on the evolution of magnetic reconnection. We have looked at both macro- and micro-scale processes, and tried to establish how these are coupled to each other. On macro-scales we have found that mass-loading reduces the reconnection rate significantly, and that this is the dominating contribution to slowing down the reconnection process in

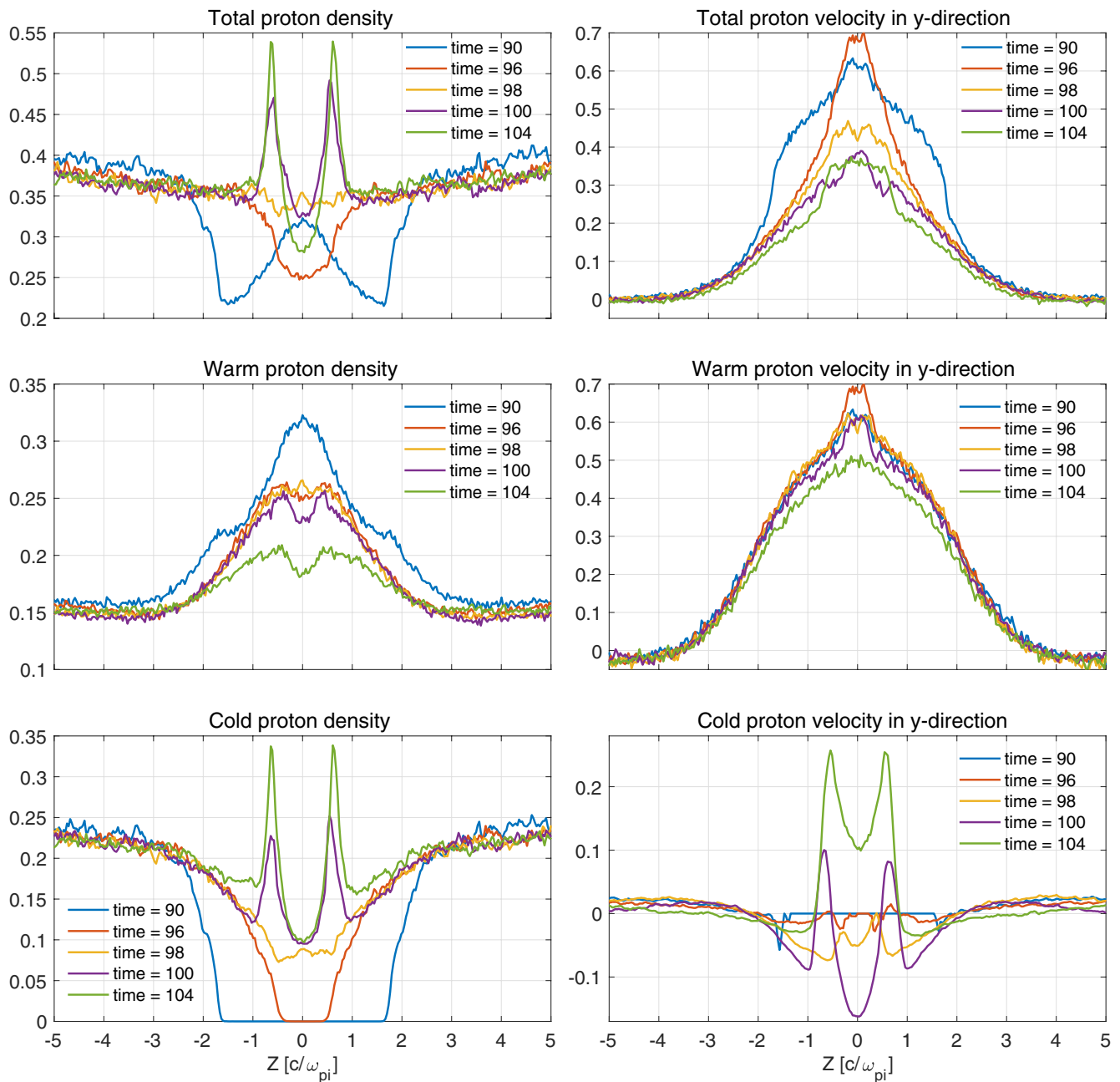


Figure 5. Density and y-directed velocity of the ion populations in the cold run as a function of z through the X-point at different times. The top row shows the total ion population, the middle row shows the warm ions and the bottom row shows the cold ions. The narrow peaks of positive velocity in the cold population results from the turning at the outer edge of their bounce motion.

this setup. We then found this reduction in the reconnection rate to be consistent with a reduction in the aspect ratio of the ion diffusion region, which is a micro-scale effect of mass-loading. Since the reconnection rate can be given as the reconnection electric field we investigated how these processes are coupled by decomposing this field to its contributing terms. We found that the cold ions carry a significant negative temporal inertia during the transition when they go from not being involved to being fully involved in the reconnection process. This transition phenomenon is only significant until the cold ions have established a sufficiently large positive diamagnetic drift to overpower the negative contribution. Through the full transition period, some cold ions will travel in the negative y -direction, opposite to both the warm ions and the cold ions that have established a diamagnetic drift. The negative temporal inertia evolves over several ion gyroperiods. This

is within the resolution of MMS (Burch et al., 2016), and both the temporary negative inertia and the counter streaming ions in the y -direction could therefore be observable as possible signatures of cold ion mass-loading in observations.

Data Availability Statement

Data for this paper is available at (Spinnangr, 2021).

Acknowledgments

The authors thank S. Toledo-Redondo for useful discussions. This study was supported by the Research Council of Norway under contract 300865, by NOTUR/NORSTOR under project NN9496K, and by NASA's MMS mission.

References

- Alm, L., André, M., Graham, D. B., Khotyaintsev, Y. V., Vaivads, A., Chappell, C. R., et al. (2019). MMS observations of multiscale Hall physics in the magnetotail. *Geophysical Research Letters*, *46*(17–18), 10230–10239. <https://doi.org/10.1029/2019GL084137>
- André, M., & Cully, C. M. (2012). Low-energy ions: A previously hidden solar system particle population. *Geophysical Research Letters*, *39*(3). <https://doi.org/10.1029/2011GL050242>
- André, M., Li, K., & Eriksson, A. I. (2015). Outflow of low-energy ions and the solar cycle. *Journal of Geophysical Research: Space Physics*, *120*(2), 1072–1085. <https://doi.org/10.1002/2014JA020714>
- André, M., Li, W., Toledo-Redondo, S., Khotyaintsev, Y. V., Vaivads, A., Graham, D. B., et al. (2016). Magnetic reconnection and modification of the Hall physics due to cold ions at the magnetopause. *Geophysical Research Letters*, *43*(13), 6705–6712. <https://doi.org/10.1002/2016GL069665>
- Burch, J. L., Moore, T. E., Torbert, R. B., & Giles, B. L. (2016). Magnetospheric multiscale overview and science objectives. *Space Science Reviews*, *199*(1–4), 5–21. <https://doi.org/10.1007/s11214-015-0164-9>
- Cassak, P. A., Liu, Y. H., & Shay, M. A. (2017). A review of the 0.1 reconnection rate problem. *Journal of Plasma Physics*, *83*(5). Cambridge University Press. <https://doi.org/10.1017/S0022377817000666>
- Comisso, L., & Bhattacharjee, A. (2016). On the value of the reconnection rate. *Journal of Plasma Physics*, *82*(6), 1–9. <https://doi.org/10.1017/S002237781600101X>
- Dargent, J., Aunai, N., Lavraud, B., Toledo-Redondo, S., & Califano, F. (2019). Signatures of cold ions in a kinetic simulation of the reconnecting magnetopause. *Journal of Geophysical Research: Space Physics*, *124*(4), 2497–2514. <https://doi.org/10.1029/2018JA026343>
- Dargent, J., Aunai, N., Lavraud, B., Toledo-Redondo, S., & Califano, F. (2020). Simulation of plasmaspheric plume impact on dayside magnetic reconnection. *Geophysical Research Letters*, *47*(4). <https://doi.org/10.1029/2019GL086546>
- Dargent, J., Aunai, N., Lavraud, B., Toledo-Redondo, S., Shay, M. A., Cassak, P. A., & Malakit, K. (2017). Kinetic simulation of asymmetric magnetic reconnection with cold ions. *Journal of Geophysical Research: Space Physics*, *122*(5), 5290–5306. <https://doi.org/10.1002/2016JA023831>
- Divin, A., Khotyaintsev, Y. V., Vaivads, A., André, M., Toledo-Redondo, S., Markidis, S., & Lapenta, G. (2016). Three-scale structure of diffusion region in the presence of cold ions. *Journal of Geophysical Research: Space Physics*, *121*(12), 12001–12013. <https://doi.org/10.1002/2016JA023606>
- Fuselier, S. A., Burch, J. L., Cassak, P. A., Goldstein, J., Gomez, R. G., Goodrich, K., et al. (2016). Magnetospheric ion influence on magnetic reconnection at the duskside magnetopause. *Geophysical Research Letters*, *43*(4), 1435–1442. <https://doi.org/10.1002/2015GL067358>
- Fuselier, S. A., Burch, J. L., Mukherjee, J., Genestreti, K. J., Vines, S. K., Gomez, R., et al. (2017). Magnetospheric ion influence at the dayside magnetopause. *Journal of Geophysical Research: Space Physics*, *122*(8), 8617–8631. <https://doi.org/10.1002/2017JA024515>
- Hesse, M., Birn, J., & Kuznetsova, M. (2001). Collisionless magnetic reconnection: Electron processes and transport modeling. *Journal of Geophysical Research: Space Physics*, *106*, 3721–3735. <https://doi.org/10.1029/1999ja001002>
- Hesse, M., Schindler, K., Birn, J., & Kuznetsova, M. (1999). The diffusion region in collisionless magnetic reconnection. *Physics of Plasmas*, *6*(5), 1781–1795. <https://doi.org/10.1063/1.873436>
- Liu, Y. H., Hesse, M., Guo, F., Daughton, W., Li, H., Cassak, P. A., & Shay, M. A. (2017). Why does steady-state magnetic reconnection have a maximum local rate of order 0.1? *Physical Review Letters*, *118*(8), 085101. <https://doi.org/10.1103/PhysRevLett.118.085101>
- Spinnangr, S. F. (2021). *Replication data for: The micro-macro coupling of mass-loading symmetric magnetic reconnection with cold ions*. DataverseNO. <https://doi.org/10.18710/NWQQBI>
- Tenfjord, P., Hesse, M., & Norgren, C. (2018). The formation of an oxygen wave by magnetic reconnection. *Journal of Geophysical Research: Space Physics*, *123*(11), 9370–9380. <https://doi.org/10.1029/2018JA026026>
- Tenfjord, P., Hesse, M., Norgren, C., Spinnangr, S. F., & Kolstø, H. (2019). The impact of oxygen on the reconnection rate. *Geophysical Research Letters*, *46*(12), 6195–6203. <https://doi.org/10.1029/2019GL082175>
- Tenfjord, P., Hesse, M., Norgren, C., Spinnangr, S. F., Kolstø, H., & Kwagala, N. (2020). Interaction of cold streaming protons with the reconnection process. *Journal of Geophysical Research: Space Physics*, *125*(6), e2019JA027619. <https://doi.org/10.1029/2019JA027619>
- Toledo-Redondo, S., André, M., Khotyaintsev, Y. V., Vaivads, A., Walsh, A., Li, W., et al. (2016). Cold ion demagnetization near the X-line of magnetic reconnection. *Geophysical Research Letters*, *43*(13), 6759–6767. <https://doi.org/10.1002/2016GL069877>
- Toledo-Redondo, S., Vaivads, A., André, M., & Khotyaintsev, Y. V. (2015). Modification of the Hall physics in magnetic reconnection due to cold ions at the Earth's magnetopause. *Geophysical Research Letters*, *42*(15), 6146–6154. <https://doi.org/10.1002/2015GL065129>
- Vasyliunas, V. M. (1975). Theoretical models of magnetic field line merging. *Reviews of Geophysics*, *13*(1), 303–336. <https://doi.org/10.1029/RG013i001p00303>
- Walsh, B. M., Foster, J. C., Erickson, P. J., & Sibeck, D. G. (2014). Simultaneous ground- and space-based observations of the plasmaspheric plume and reconnection. *Science*, *343*(6175), 1122–1125. <https://doi.org/10.1126/science.1247212>
- Yamada, M., Kulsrud, R., & Ji, H. (2010). Magnetic reconnection. *Reviews of Modern Physics*, *82*(1), 603–664. <https://doi.org/10.1103/RevModPhys.82.603>